Atmospheric
Chemistry
and Physics
Discussions

Open Access

EGU

Bridging the condensation-collision size gap: a direct numerical simulation of continuous droplet growth in turbulent cloud

Sisi Chen[1], Man-Kong Yau[1], Peter Bartello[1], and Lulin Xue[2]

[1]McGill University, Montréal, Québec, Canada
[2]National Center for Atmospheric Research, Boulder, Colorado, USA

Correspondence: Sisi Chen (sisi.chen@mail.mcgill.ca)

Abstract. In most previous DNS studies on droplet growth in turbulence, condensational growth and collisional growth were treated separately. Studies in recent decades have postulated that small-scale turbulence may accelerate droplet collisions when droplets are still small when condensational growth is effective. This implies that both processes should be considered simultaneously to unveil the full history of droplet growth and rain formation. This paper introduces the first DNS approach

5   to explicitly study the continuous droplet growth by condensation and collisions inside an adiabatic ascending cloud parcel. Results from the condensation-only, collision-only, and condensation-collision experiments are compared to examine the contribution to the broadening of droplet size distribution by the individual process and by the combined processes. Simulations of different turbulent intensities are conducted to investigate the impact of turbulence on each process and on the condensation-induced collisions. The results show that the condensational process promotes the collisions in a turbulent environment and

10   reduces the collisions when in still air, indicating a positive impact of condensation on turbulent collisions. This work suggests the necessity to include both processes simultaneously when studying droplet-turbulence interaction to quantify the turbulence effect on the evolution of cloud droplet spectrum and rain formation.

1   Introduction

Theoretical studies indicate that for droplets in the size range of 15-30μm in radius, referred to as the condensation-collision

15   size gap, neither condensational growth nor collisional growth is effective(Pruppacher and Klett, 1997) in producing precipitation. Classical parcel models generally yielded very narrow droplet size distributions (DSDs) and take a rather long time to form rain (Jonas, 1996). In nature, wide DSDs and large droplets are frequently observed in cumulus and even statocumulus clouds (e.g., Brenguier and Chaumat, 2001; Pawlowska et al., 2006; Prabha et al., 2012). This size gap problem represents a longstanding challenge in the ongoing quest to understand the warm-rain initiation process. In the literature, various mech-

20   anisms have been proposed to accelerate rain development, such as small-scale turbulence (Vaillancourt and Yau, 2000), the presence of giant aerosols (Johnson, 1982; Blyth et al., 2003; Jensen and Nugent, 2017), entrainment of unsaturated air (Baker et al., 1980; Lasher-trapp et al., 2005; Cooper et al., 2013) and large-eddy hopping (Cooper, 1989; Grabowski and Abade, 2017). This study focuses on the effect of small-scale turbulence containing eddies in the inertial-dissipative range with length-

Atmospheric
Chemistry
and Physics
Discussions

scales ≪ 10 m as shown in Fig. 1 of Grabowski and Wang (2013) which can be resolved by the technique of direct numerical simulation (DNS).

Several mechanisms related to turbulence have been proposed to explain the fast growth of droplets in the condensation-collision size gap (Grabowski and Wang, 2013; Devenish et al., 2012). As a result of the response of droplet inertia to the turbulent eddies of different scales, turbulent flow creates two effects: the non-uniform distribution of cloud droplets (clustering effect) and increase in the relative velocities between droplets (transport effect). A number of DNS studies have reported that the geometric collision rate of droplets increases as turbulence intensifies (Franklin et al., 2005; Ayala et al., 2008; Onishi and Seifert, 2016). Concomitantly, turbulence modifies the response of a droplet to the local disturbance flow induced by other droplets through hydrodynamic interactions to increase the collision efficiency (Wang et al., 2008; Onishi et al., 2013; Chen et al., 2018). In particular, Chen et al. (2018) demonstrated that the turbulence enhancement on collisions became most significant among droplet pairs of similar sizes, suggesting that turbulence may efficiently broaden the narrow DSD generated from condensational growth.

Moreover, it has also been argued that the supersaturation perturbation field can arise from the fluctuation of temperature and water vapor in turbulence and the differential local water vapor consumption (a.k.a. Srivastava effect, Srivastava, 1989) enhanced by droplet clustering. This may lead to a distinct growth history by condensation for each droplet as it is transported in a turbulent flow (Lanotte et al., 2009). However, several DNS studies found that small-scale turbulence can only create small, if not insignificant, drop size broadening through condensation (Vaillancourt et al., 2002; Lanotte et al., 2009; Sardina et al., 2015). The reason is that the average time that droplets are exposed to supersaturation perturbations shortens as the turbulence intensifies and as droplets grow larger to begin to sediment (Vaillancourt et al., 2002). Lanotte et al. (2009) reported a wider size distribution when the Reynolds number of the flow (i.e., the computational domain size) increased from 40 to 185 and proposed a simple scaling to extrapolate the DNS result to the typical size of a cloud adiabatic core (approximately 100 m wide or Reynolds number ≈ 5000). However, cautions should be exercised to apply this scaling as DNS is not able to capture the spatiotemporal complexity of the turbulence at much larger scales beyond the size of the domain. Sardina et al. (2015) also used a similar model as Lanotte et al. (2009) but extended the simulation time to 20 minutes to be comparable to the formation time of rain revealed in real observation. They found that the variance of the droplet size distribution was mainly determined by the large-scale flow. Nevertheless, it should be noted that their conclusion was based on the simplified assumption that both the mean updraft speed and the mean supersaturation were zero. On the other hand, the DNS model of Toshiyuki et al. (2016) considered a time-dependent and buoyancy-driven mean vertical motion calculated from a given environmental sounding. In their study of the effect of turbulence and entrainment on the evolution of cloud droplets, it was found that the thermodynamic fluctuations caused by turbulent advection prevented the buildup of the buoyancy force, leading to an even slower evolution of the mean droplet size and the vertical velocity as compared to those predicted by a parcel model.

A common limitation shared by most, if not all, previous DNS studies is that, the condensation process and collision-coalescence process were studied separately. This assumption may be justifiable in a parcel model due to the non-overlapping droplet-size regimes of the two growth processes in still-air. However this assumption is questionable in DNS studies which reveal substantial turbulent enhancement of collision among droplets in the condensation-collision size gap. As there is an

absence of DNS work on continuous droplet growth incorporating both processes, it is the goal of this study to unveil the full history of droplet growth and DSD broadening by condensational and collisional growth in a turbulent, supersaturated environment in an adiabatic ascending process.

The purpose of this study is: 1) to introduce the first DNS approach to explicitly resolve the continuous droplet growth by condensation and collision in shallow, turbulent clouds, and 2) to answer the following two questions: "how does the droplet collisional process interact with the droplet condensational growth process?" and "what is the role of turbulence in this interaction? "

Our approach is to incorporate the droplet hydrodynamic collision and condensation processes into a single DNS modeling framework. Arguably, this model provides a first direct approach to bridge the condensation-collision gap that has puzzled the cloud physics community for decades.

The paper is organized as follows. In Sect. 2 we describe the sets of equations adopted from Vaillancourt et al. (2001) and Chen et al. (2018) and the accompanying modification. The simulated results from three sets of experiments (condensation-only, collision-only, condensation-collision) in various turbulent environments are given in Sect. 3, to be followed by a conclusion and remarks on the limitation of this study in Sect. 4.

2 Model description and experimental setup

This paper represents a sequel to Chen et al. (2018) as part of our on-going exploration of the evolution of cloud DSD affected by turbulence. The DNS model adopted was originally developed by Vaillancourt et al. (2001) in perhaps one of the earliest DNS approaches to simulate droplet growth in turbulence. Vaillancourt et al. (2001) focused on the impact of turbulence on droplet condensation, and thus collisions were not considered. A number of extension followed. Franklin et al. (2005) resolved the droplet collisions using an efficient collision detection technique. Chen et al. (2016) made changes to allow simulation in larger domain sizes and introduced a new forcing scheme to achieve a statistically steady turbulent dissipation rate. Chen et al. (2018) added the local disturbance flow field induced by droplets to obtain accurate turbulent collision efficiencies and droplet collisional growth affected by both the disturbance flow and the turbulence flow.

In the present study, the model from Chen et al. (2018) is further extended to restore the thermodynamics framework of Vaillancourt et al. (2001) to include condensational growth. Specifically, the whole DNS box is regarded as a parcel ascending adiabatically from near the cloud base with a constant mean updraft. Two sets of equations are used to solve for 1) the macroscopic variables that describe the time evolution of the parcel mean state properties and 2) the microscopic variables that describe the turbulent flow, as well as the temperature and the water vapor mixing ratio fluctuation fields. Furthermore, equations pertaining to the thermodynamics process are modified to improve the accuracy of droplet condensational growth. For convenience of reference, the detailed equations are provided in Appendix B.

In the presence of the thermodynamic fluctuation fields and the turbulence flow field, droplets grow in two distinct ways simultaneously:

Atmospheric
Chemistry
and Physics
Discussions

1) Droplets grow by condensation with its growth rate directly proportional to the instantaneous supersaturation (see Eq. (B1) in Appendix B). When a droplet moves relative to the air, the water vapor field is not spherically symmetric around the droplet surface but is modified depending on the direction of motion (so-called the ventilation effect). This effect becomes important when droplets are greater than 30 μm in radius (Sedunov, 1974). In Vaillancourt et al. (2001), all droplets were smaller than 20 μm and this effect was not considered. However, the present study allows droplet to grow larger and thus a ventilation coefficient is added to the droplet growth equation. Following Vaillancourt et al. (2001), the curvature term and the solute term are neglected in the equation, and the droplets are treated as pure water drops since all droplets in this study are greater than 5 μm (Pruppacher and Klett, 1997).

2) Simultaneously, droplets grow through the collision-coalescence process. The droplet motion and collisional growth are treated in the same manner as in Chen et al. (2018). Each droplet is tracked in the Lagrangian framework, with its motion determined by the gravity and the local fluid drag force (Eq.(1) in Chen et al., 2018). Once two droplets collide, they coalesce to become a bigger entity with its mass equal to the sum of the masses of the collided droplets and its location being the barycenter of the binary system before the collision. The velocity of the coalesced droplet is calculated based on the conservation of momentum. Since we are particularly interested in the condensation-collision size range ($r \ll 100\ \mu m$) and solving the motion of droplets over 100 μm requires more complex consideration such as turbulent wakes induced and drop deformation which are beyond the scope of this study, droplets reaching 100 μm are considered as fall-outs and are not allowed to grow further, i.e., they neither interact with other droplets nor affect the local disturbance flows.

Three sets of experiments are conducted to evaluate the DSD broadening due to the turbulence effect on different droplet growth processes: 1) droplet growth by condensation only (referred to as the condensation-only experiment), 2) droplet growth by collision-coalescence only (referred to as the collision-only experiment), and 3) droplet growth by condensation and collision-coalescence together (referred to as the condensation-collision experiment), respectively. All experiments use the same initial DSD shape adopted from an aircraft measurement in non-precipitating cumulus clouds (Raga et al., 1990). The initial droplet number concentration is set as 80 cm^{-3} and a constant updraft of 2.5 m/s is used to represent the condition of pristine maritime cumulus clouds.

For each set of experiment (except for the condensation-only experiment), three flow configurations are considered: purely-gravitational case (i.e., still air), weak turbulence case (with eddy dissipation rate $\epsilon = 50\ cm^2 s^{-3}$), and strong turbulence case (with $\epsilon = 500\ cm^2 s^{-3}$). The domain size of each simulation is about 10 cm in each direction, with grid space ≈ 0.1 cm determined by the dissipation rate as explained in Chen et al. (2016). It is recognized that droplet condensation in still-air leads to a narrow DSD and DSD broadening by condensation impacted by small-scale turbulence is insignificant. Therefore, during the condensation-only experiment, only the strong turbulence simulation is performed to serve as an upper bound of the DSD broadening among the three flow conditions. As a result, seven simulations are performed. Each simulation lasts 6.5 minutes of real-time which is the approximate duration for the whole parcel to ascend from cloud base to 1000 m above the base, representing a typical cumulus development.

3 Result and discussion

We first compare the results from the three experiments to scrutinize the contributions of the different droplet growth processes under the effect of turbulence. Figure 1 shows the DSDs at the end of each experiment in strong turbulence condition. As a reference, the initial DSD is displayed with a gray area. Consistent with past findings, the turbulence effect on droplet conden-

5   sational growth is small. The condensation-only process produces the narrowest size distribution among the three experiments and droplets grow no larger than 20 μm at the end of the simulation. On the other hand, in both the collision-only experiment (blue curve) and the condensation-collision experiment (yellow curve), a substantial number of large droplets are found. Furthermore, compared to the collision-only simulation, the condensation-collision experiment generates more large droplets and substantially larger droplets. The largest r reaches 100 μm at the end of the simulation compared to less than 65 μm in the

10   collision-only case. Meanwhile, the number concentration of r > 30 μm droplets in the condensation-collision case increases by a factor of 2.3 (0.35 cm^{-3} compared to 0.15 cm^{-3} in the collision-only case).
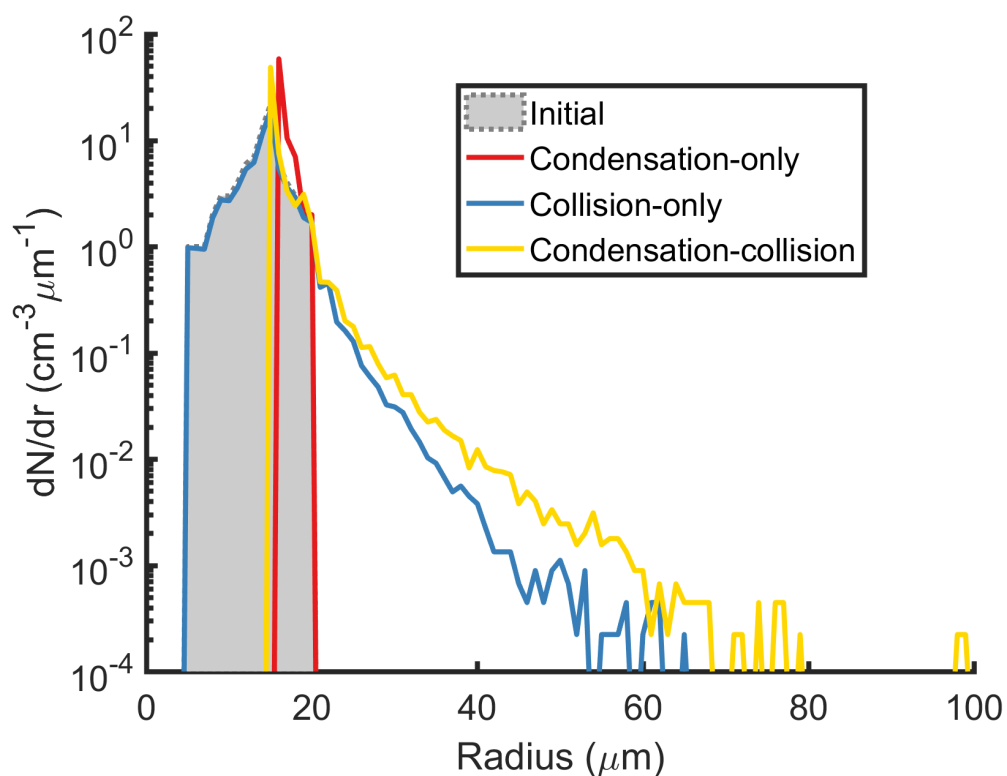

Figure 1. Droplet size distributions at the 6.5th minute for condensation only case (red), collision only case (blue) and condensation-collision case (yellow). Dissipation rate is 500 $cm^2 s^{-3}$ for all cases with the initial size distribution shown as a dashed grey line.

To examine whether this enhanced broadening due to the inclusion of condenational process depends on the flow conditions, detailed comparisons between the collision-only and the condensation-collision experiments are made under three flow conditions: purely-gravitational, weak turbulence, and strong turbulence. Figure 2 demonstrates the time evolution of DSD in the two sets of experiments under the three different flows. It is found that:

5   1) In the purely-gravitational case (Figs. 2(a) and 2(b)), despite the condensation-collision experiment producing larger maximum droplets at the end of the simulation relative to the collision-only experiment (black outline in Fig. 2), the number concentration of large droplets is still negligible (as $r > 35 \ \mu m$ droplets stay below $0.001 \ cm^{-3}$ as seen from the expansion of the purple edge with time);

2) In the turbulence cases, we observe more large droplets and much larger maximum droplet sizes in the domain when
10   condensational growth is considered. With weak turbulence, droplets larger than 35 μm (over $0.001 \ cm^{-3}$) can be seen as early as 3.5 minutes in the condensation-collision experiment, but 6 minutes in the collision-only run. With strong turbulence, large droplets were found in the 3rd minute in the condensation-collision simulation compared to the 4th minute without condensation. It is evidence that both experiments experience earlier formation of large droplets as turbulence intensifies while the inclusion of condensation further accelerate the droplet growth. This result evinces that an effective turbulence-impacted
15   condensation-collision broadening mechanism exists that strengthened with increasing turbulence intensity.

A condensation-induced broadening has been found in all three flow conditions, though it seems that such broadening is negligible in the case of still air. This phenomenon can be explained by two main mechanisms:

1) The condensational growth process effectively grows droplets of small sizes ($r < 10 \ \mu m$) to medium size ($10 - 20 \ \mu m$) due to the fast growth rate of small droplets. This conjecture is supported by the result on the right column of Fig. 2 showing
20   that among the three condensational cases, all droplets smaller than 15 μm become greater than 15 μm within 4 minutes. As bigger droplets have higher collision rates, the average collision rate in the domain is expected to increase progressively as more medium-sized droplets are formed through condensation, and they become more likely to be collected by other droplets.

2) Condensational growth dynamically narrows the DSD and providing a great number of similar-sized droplets (i.e., the radius ratio between the small droplet and large droplet, r/R, is close to unity). Chen et al. (2018) found that turbulence
25   enhancement on collision rate is most significant in similar-sized droplets, and stays relatively weak for $0.2 < r/R < 0.8$ (Fig. 3 in their paper). In an environment with similar-sized droplets created by condensation, the turbulence-enhanced collisions are enhanced to accelerate the production of large droplets.

The first mechanism of enhanced collision rate due to larger mean droplet sizes can also happen in purely-gravitational case but will be offset by the inefficient gravitational collection process due to DSD narrowing by condensation. In turbulence
30   cases, the condensational DSD produce similar-sized droplets to allow the turbulence-enhanced similar-sized collision process to act, leading to a positive feedback mechanism. Evidence for this hypothesis can be found by comparing the probability distribution function (PDF) of collisions with respect to r/R (the radius ratio between the small droplet and big droplet in a droplet pair) in the collision-only and the collision-condensation experiments. As seen in Fig. 3, the PDF of collisions in either the weak turbulence or the strong turbulence cases become more flattened when condensation is included. In particular, the
35   chance of similar-sized collisions ($r/R > 0.9$) is substantially greater. On the contrary, a narrower PDF is observed in the
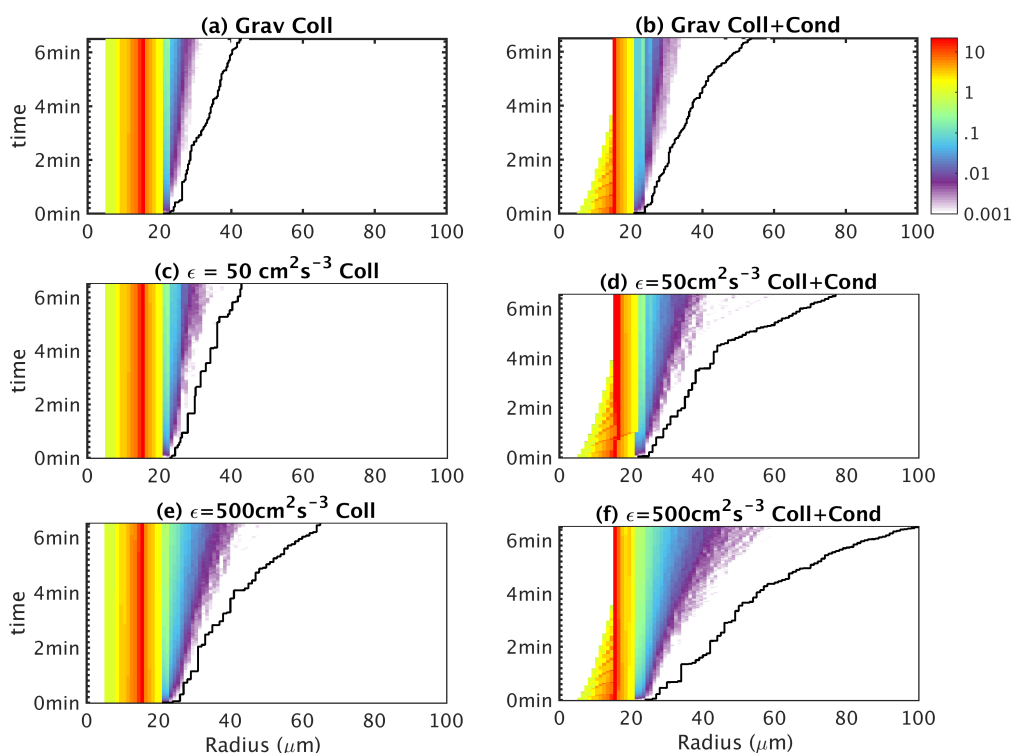
Figure 2. The time evolution of DSD in the collision-only experiments (left column) and the collision-condensation experiments (right column). Results from the purely-gravitational case (first row), weak turbulence ($\epsilon = 50\ cm^2 s^{-3}$, second row), and strong turbulence ($\epsilon = 500\ cm^2 s^{-3}$, third row) are demonstrated. The solid black curve indicates the largest droplet of the entire domain. The droplet number concentration (cm^{-3}) on each size bin (bin width = 1 μm) is displayed in color using a logarithmic scaling shown in the color bar. Droplet number concentrations below 0.001 cm^{-3} are treated as statistical uncertainty since they correspond to less than 2-4 droplets in the domain and thus are given no color in the plot.

purely-gravitational case (Figs. 3(a) and 3(b)). Figure 4 demonstrates the distributions of collision frequency and the collision enhancement due to condensation. It is found that in the purely-gravitational case the number of similar-sized collisions doubles in the condensation-collision experiment, which results from the increased number of similar-sized droplets introduced by condensation. It is obvious that increasing the intensity of turbulence further enhances these collisions. The similar-sized collisions increase by a factor of 3.5 in weak turbulence and a factor of 4.5 in strong turbulence.

In the small r-ratio range ($r/R < 0.7$), the total collisions in the purely-gravitational case are lowered by more than half due to a declined number of those droplet pairs (Fig. 4(g)). However, in the turbulent cases, the collision frequency instead experiences a mild increase compared to the collision-only experiment. This increase is due to the fact that condensational process increases the population of medium-sized droplets ($r = 10-20\mu m$) and turbulence continues to enhance the collisions of these droplets.

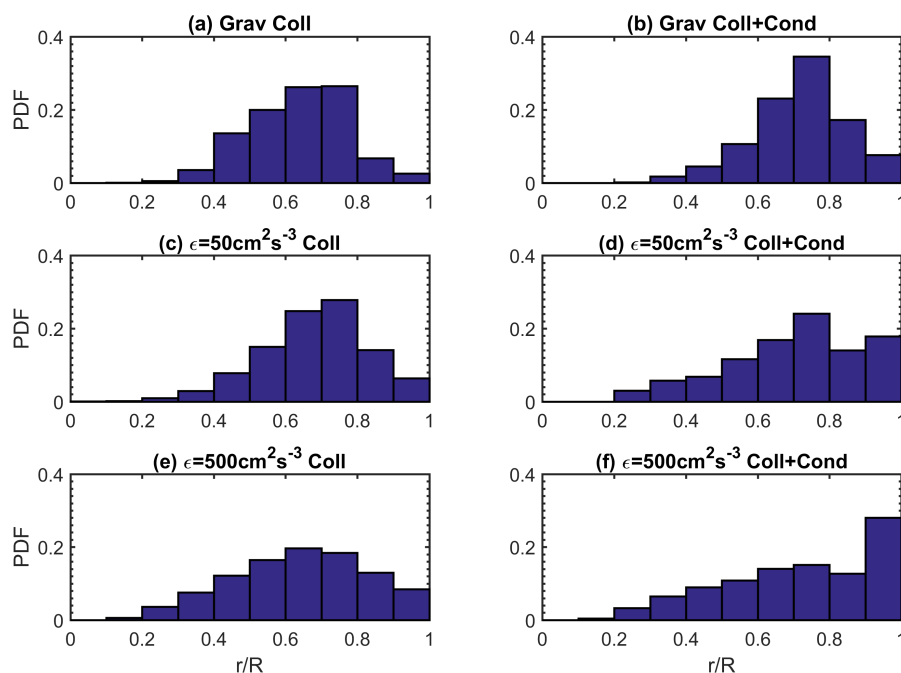Atmospheric
Chemistry
and Physics
Discussions

Figure 3. Probability distribution function (PDF) of collisions with respect to r/R at three different flow conditions (first row: pure gravity, second row: weak turbulence, third row: strong turbulence). Results from the collision-only experiments (the left column) and the condensation-collision experiments (the right column) are shown for comparison

The abundant number of those medium-sized droplets boost the number of similar-sized collisions by turblence to produce larger droplets. Meanwhile, the larger size from growth by condensation substantially increases the chance of those droplets to be collected by other larger droplets. Furthermore, the formation of large droplets due to the turbulence-enhanced collisions in turn contributes to the growing collector droplet population, thus further increasing the chance of these medium-sized droplets

5   to be collected. In the purely gravitational case, this process is inhibited by the insignificant similar-sized collisions in spite of their number being doubled from the collisional-only case.

4   Conclusions

This work provides a first DNS study to explicitly resolve continuous droplet growth by condensation and collision in a turbulent environment. The results are expected to contribute toward resolving the warm-rain initiation problem.

10   Results from the condensation-only, collision-only, and condensation-collision experiments are compared to examine the contribution to the DSD broadening by the individual process and by the combined processes acting in concert. Three different flow environments (still air, weak turbulence, and strong turbulence) are investigated to scrutinize the impact of turbulence
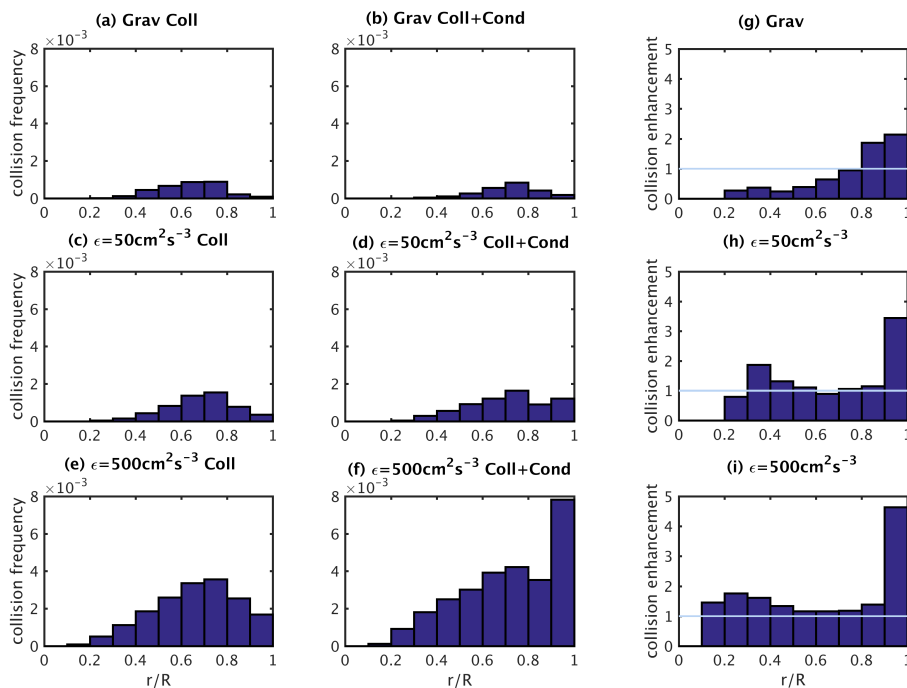
Atmospheric
Chemistry
and Physics
Discussions

Figure 4. Subplot (a)-(f) are same as Fig. 3 but for the collision frequency $(cm^{-3}s^{-1})$ from different r/R pairs. Subplot (g)-(i) are the enhancement of collision frequency for different r/R pairs due to the inclusion of condensation. The enhancement is calculated by taking the ratio of the collision frequency from the condensation-collision experiment and the collision-only experiment. Results from three different flow conditions are demonstrated.

in the condensational-induced collisions. By comparing the collision frequencies of the collision-only experiment and the condensation-collision experiment, it is found that condensational growth boosts the collisions when the flow is turbulent and slows down the collisions for the case of still air.

In the purely-gravitational experiment, the abundant similar-sized droplets generated by condensation inhibit the gravitational collection process, and the collision frequency of $r/R < 0.7$ reduces by half. As a result, the number concentration of droplet larger than 35 μm remains lower than 0.001 cm^{-3} throughout the simulation.

In the turbulence experiments, a greater number of large droplets are observed, and their appearance occurs faster as turbulence intensifies, implying an effective turbulence impact on droplet size broadening. Furthermore, droplets larger than 35 μm form 1-2 minutes earlier in the collision-condensation experiments. It follows that these droplets can be observed as early as the 3rd minute in strong turbulence situation. This result suggests that a sophisticated model that takes into account both the turbulence-enhanced collisions and condensational-induced collisions under the effect of turbulence should be used to study the cloud droplet spectrum broadening and rain formation.

Atmospheric
Chemistry
and Physics
Discussions

Finally we remark on the limitation of this study and some suggestions for the future work. It has been found that the evolution of the DSD and the rain formation time highly depend on the initial shape of DSD and the droplet number concentration. Therefore, simulations of different initial DSDs are to be conducted to better understand its dependency. In addition, the initial DSD used in this study is taken from the flight observation which is an average over a long sampling time and a wide sampling

5 space. In this case, the initial DSD is not guaranteed to be representative of the steady-state DSD from aerosol activation and condensational growth in cloud adiabatic cores. However, with the continuous advancement of the in-situ measurement technology such as HOLO-DEC (Glienke et al., 2017), instantaneous sampling that accurately represents the DSD near the cloud base inside adiabatic cores can be possible in the near future. For a more realistic representation of an early stage DSD, the aerosol activation process should be included to enable cloud particles to grow from the very beginning (i.e., dry aerosols in

10 sub-cloud regions). We strive to explore this approach in a future study.

Appendix A: List of constants

See list of constants in Table A1

Table A1. List of constants

$D_v = 2.55 \times 10^{-5}$	water vapor diffusivity $[m^2 s^{-1}]$
$D_t = 2.22 \times 10^{-5}$	thermal diffusivity $[m^2 s^{-1}]$
$\nu = 1.6 \times 10^{-5}$	air kinematic viscosity $[m^2 s^{-1}]$
$K_a = 2.48 \times 10^{-2}$	thermal conductivity of air $[Jm^{-1}s-1K^{-1}]$
$R_v = 461.5$	Individual gas constant for water vapour $[JKg^{-1}K^{-1}]$
$R_a = 287$	Individual gas constant for dry air $[JKg^{-1}K^{-1}]$
$L = 2.477 \times 10^6$	specific latent heat for water $[JKg^{-1}K^{-1}]$
$C_p = 1005$	specific heat for air $[JKg^{-1}K^{-1}]$
$\Gamma_d = -g/C_p$	dry adiabatic lapse rate
$\rho_w = 1000.0$	density of water $[Kgm^{-3}]$
$S_{ch} = \nu/D_v$	Schmidt number

Appendix B: Equations for DNS model

B1   Microscopic equations

15 The condensational growth rate of an individual droplet with radius R_i is as follow:

$$\frac{dR_i}{dt} = 2K f_v S. \tag{B1}$$

Here $K^{-1} = \frac{\rho_w R_v T}{e_{sat}(T) D_v} + \frac{L\rho_w}{K_a T}(\frac{L}{R_v T} - 1)$, where e_{sat} is the saturated water vapor pressure. f_v refers to the droplet ventilation coefficient. The value of f_v is determined by the empirical formulas from laboratory experiment of Beard and Pruppacher (1971):

$$f_v = 1.0 + 0.108(N_{Sc}^{1/3} Re_p^{1/2})^2, \text{ for } N_{Sc}^{1/3} Re_p^{1/2} < 1.4, \tag{B2}$$

5

$$f_v = 0.78 + 0.308(N_{Sc}^{1/3} Re_p^{1/2}), \text{ for } 51.4 > N_{Sc}^{1/3} Re_p^{1/2} \geq 1.4, \tag{B3}$$

where $Re_p = \frac{2R_i|\mathbf{V}|}{\nu}$ is the droplet Reynolds number, $\mathbf{V}$ is the velocity of droplet i. S is the supersaturation in the grid cell where droplet i is located, defined as

$$S = \frac{q_v}{q_{vs}} - 1, \tag{B4}$$

10   where q_v is the water vapor mixing ratio, with its corresponding saturated value q_{vs} determined by temperature ((2.17)-(2.18) in Rogers and Yau 1989). We assume that all droplets residing in the same grid cell are exposed to the same supersaturation environment. The scaler fields of q_v and temperature T can be decomposed into the parcel mean state and the perturbation state. The parcel mean state is calculated via the macroscopic set of equations shown in Sect. B2 and the perturbations are calculated as follows:

15
$$\frac{\partial T'}{\partial t} = -\nabla \cdot (\mathbf{U}T') - W'\Gamma_d + \frac{L}{C_p}C_d' + D_t\nabla^2 T', \tag{B5}$$

$$\frac{\partial q_v'}{\partial t} = -\nabla \cdot (\mathbf{U}q_v') - C_d' + D_v\nabla^2 q_v', \tag{B6}$$

where W' is the vertical perturbation velocity. $C_d' = C_d - C_{dM}$ is the differential condensation rate between the grid cell and the whole parcel. Given (B1), the condensation rate inside the grid cell can be simplified as:

20
$$C_d = \frac{1}{m_a}\sum_i^n \frac{4}{3}\pi\rho_w \frac{dR_i^3}{dt} = \frac{4}{m_a}\pi\rho_w K f_v \sum_i^n R_i S. \tag{B7}$$

The turbulent velocity field $\mathbf{U}$ is governed by the incompressible Navier-Stokes equations:

$$\frac{\partial \mathbf{U}}{\partial t} + (\mathbf{U} \cdot \nabla)\mathbf{U} = -\frac{1}{\rho_a}\nabla P + \nu\nabla^2\mathbf{U} + \mathbf{F}, \tag{B8}$$

$$\nabla \cdot \mathbf{U} = 0, \tag{B9}$$

25   where P is the perturbation pressure deviated from the hydrostatic pressure P_M. The pressure term can be dropped when the equations are solved in the vorticity form. $\mathbf{F}$ is the external forcing. We used the forcing method of Sullivan et al. (1994)

to maintain the turbulence. A simple modification to the forcing scheme by Chen et al. (2016) is introduced to improve the efficiency in obtaining the desired mean dissipation rates. The droplet motion is governed by fluid drag force and gravity:

$$\frac{d\mathbf{V}(t)}{dt} = \frac{\mathbf{V}(t) - \tilde{\mathbf{U}}(\mathbf{X}(t),t)}{\tau_p} + \mathbf{g}, \tag{B10}$$

τ_p denotes the droplet response time. For $r < 40\mu m$, Stokes drag force is applied and $\tau_p = (\frac{2\rho_w}{9\nu\rho_a})r^2$. Droplet terminal velocity
5 can be obtained using $V_T = g\tau_p$. For $r \geq 40\mu m$, the terminal velocity derived from the experimental data is applied to those big droplets: $V_T = k_2 r$, here $k_2 = 8 \times 10^3 s^{-1}$ (Rogers and Yau, 1989, p.126). $\tilde{\mathbf{U}}$ is the flow velocity at the droplet center, contributed by the turbulent flow field $\mathbf{U}$ and the disturbance flow $\mathbf{U_{dist}}$ caused by neighboring droplets (Chen et al., 2018). The superposition method by Wang et al. (2005) is used to calculate the disturbance flow.

B2 Macroscopic equations

10 The time evolution of the parcel-mean temperature T_M, water vapor mixing ratio q_{vM}, pressure P_M, density ρ_{aM} are described as below. All variables of parcel mean are denoted with a subscript M.

$$\frac{dT_M}{dt} = -W_M\Gamma_d + \frac{L}{C_p}C_dM \tag{B11}$$

$$\frac{dq_{vM}}{dt} = -C_{dM} \tag{B12}$$

15

$$C_{dM} = \frac{1}{M_a}\sum_i^N \frac{d}{dt}\left(\frac{4}{3}\pi\rho_w R_i^3\right) = \frac{4}{M_a}\pi\rho_w K f_v \sum_i^N R_i S, \tag{B13}$$

$$\frac{P_M}{dt} = -\rho_{aM} g W_M \tag{B14}$$

20 $$\rho_{aM} = \frac{P_M}{R_a T_M} \tag{B15}$$

The total fields of T and q_v are calculated by adding the macroscopic variables and the perturbation variables.

Competing interests. The authors declare that they have no conflict of interest.

Atmospheric
Chemistry
and Physics
Discussions

References

Ayala, O., Rosa, B., Wang, L.-P., and Grabowski, W. W.: Effects of turbulence on the geometric collision rate of sedimenting droplets. Part 1. Results from direct numerical simulation, New J. Phys., 10, 075 015, 2008.

Baker, M., Corbin, R., and Latham, J.: The influence of entrainment on the evolution of cloud droplet spectra: I. A model of inhomogeneous mixing, Quart. J. Roy. Meteor. Soc., 106, 581–598, 1980.

Blyth, A. M., Lasher-Trapp, S. G., Cooper, W. A., Knight, C. A., and Latham, J.: The role of giant and ultragiant nuclei in the formation of early radar echoes in warm cumulus clouds, J. Atmos. Sci., 60, 2557–2572, 2003.

Brenguier, J.-L. and Chaumat, L.: Droplet Spectra Broadening in Cumulus Clouds. Part I: Broadening in Adiabatic Cores, J. Atmos. Sci., 58, 628–641, 2001.

Chen, S., Bartello, P., Yau, M. K., Vaillancourt, P. A., and Zwijsen, K.: Cloud Droplet Collisions in Turbulent Environment: Collision Statistics and Parameterization, J. Atmos. Sci., 73, 621–636, 2016.

Chen, S., Yau, M. K., and Bartello, P.: Turbulence effects of collision efficiency and broadening of droplet size distribution in cumulus clouds, J. Atmos. Sci., https://doi.org/10.1175/JAS-D-17-0123.1, 2018.

Cooper, W. A.: Effects of variable droplet growth histories on droplet size distributions. Part I: Theory, J. Atmos. Sci., 46, 1301–1311, 1989.

Cooper, W. A., Lasher-Trapp, S. G., and Blyth, A. M.: The influence of entrainment and mixing on the initial formation of rain in a warm cumulus cloud, J. Atmos. Sci., 70, 1727–1743, 2013.

Devenish, B. J., Bartello, P., Brenguier, J. L., Collins, L. R., Grabowski, W. W., Ijzermans, R. H. A., Malinowski, S. P., Reeks, M. W., Vassilicos, J. C., Wang, L. P., and Warhaft, Z.: Droplet growth in warm turbulent clouds, Quart. J. Roy. Meteor. Soc., 138, 1401–1429, 2012.

Franklin, C. N., Vaillancourt, P. A., Yau, M. K., and Bartello, P.: Collision Rates of Cloud Droplets in Turbulent Flow, J. Atmos. Sci., 62, 2451–2466, 2005.

Glienke, S., Kostinski, A., Fugal, J., Shaw, R. A., Borrmann, S., and Stith, J.: Cloud droplets to drizzle: Contribution of transition drops to microphysical and optical properties of marine stratocumulus clouds, Geophys. Res. Lett., 44, 8002–8010, 2017.

Grabowski, W. W. and Abade, G. C.: Broadening of Cloud Droplet Spectra through Eddy Hopping: Turbulent Adiabatic Parcel Simulations, J. Atmos. Sci., 74, 1485–1493, 2017.

Grabowski, W. W. and Wang, L.-P.: Growth of Cloud Droplets in a Turbulent Environment, Annu. Rev. Fluid Mech., 45, 293–324, 2013.

Jensen, J. B. and Nugent, A. D.: Condensational Growth of Drops Formed on Giant Sea-Salt Aerosol Particles, J. Atmos. Sci., 74, 679–697, 2017.

Johnson, D. B.: The role of giant and ultragiant aerosol particles in warm rain initiation, J. Atmos. Sci., 39, 448–460, 1982.

Jonas, P.: Turbulence and cloud microphysics, Atmos. Res., 40, 283 – 306, 1996.

Lanotte, A. S., Seminara, A., and Toschi, F.: Cloud Droplet Growth by Condensation in Homogeneous Isotropic Turbulence, J. Atmos. Sci., 66, 1685–1697, 2009.

Lasher-trapp, S. G., Cooper, W. A., and Blyth, A. M.: Broadening of droplet size distributions from entrainment and mixing in a cumulus cloud, Quart. J. Roy. Meteor. Soc., 131, 195–220, 2005.

Onishi, R. and Seifert, A.: Reynolds-number dependence of turbulence enhancement on collision growth, Atmospheric Chemistry and Physics, 16, 12 441–12 455, 2016.

Onishi, R., Takahashi, K., and Vassilicos, J. C.: An efficient parallel simulation of interacting inertial particles in homogeneous isotropic turbulence, Journal of Computational Physics, 242, 809–827, 2013.

Pawlowska, H., Grabowski, W. W., and Brenguier, J.-L.: Observations of the width of cloud droplet spectra in stratocumulus, Geophys. Res. Lett., 33, 2006.

5   Prabha, T. V., Patade, S., Pandithurai, G., Khain, A., Axisa, D., Pradeep-Kumar, P., Maheshkumar, R. S., Kulkarni, J. R., and Goswami, B. N.: Spectral width of premonsoon and monsoon clouds over Indo-Gangetic valley, Journal of Geophysical Research: Atmospheres, 117, 2012.

Pruppacher, H. and Klett, J.: Microphysics of Clouds and Precipitation: With an Introduction to Cloud Chemistry and Cloud Electricity, Kluwer Acad., Norwell, Mass, 2nd edn., 1997.

10 Raga, G. B., Jensen, J. B., and Baker, M. B.: Characteristics of Cumulus Band Clouds off the Coast of Hawaii, J. Atmos. Sci., 47, 338–356, 1990.

Rogers, R. R. and Yau, M. K.: A Short Course in Cloud Physics, Butterworth-Heinemann, 3rd edn., 1989.

Sardina, G., Picano, F., Brandt, L., and Caballero, R.: Continuous Growth of Droplet Size Variance due to Condensation in Turbulent Clouds, Phys Rev Lett, 115, 184 501, 2015.

15 Sedunov, I.: Physics of drop formation in the atmosphere, vol. 22094, Halsted Press, 1974.

Srivastava, R. C.: Growth Of Cloud Drops by Condensation: A Criticism of Currently Accepted Theory and a New Approach, J. Atmos. Sci., 46, 869–887, 1989.

Sullivan, N. P., Mahalingam, S., and Kerr, R. M.: Deterministic forcing of homogeneous, isotropic turbulence, Phys. Fluids (1994-present), 6, 1612–1614, 1994.

20 Toshiyuki, G., Tamotsu, S., and Izumi, S.: Continuous growth of cloud droplets in cumulus cloud, New J. Phys., 18, 043 042, 2016.

Vaillancourt, P. A. and Yau, M. K.: Review of Particle-Turbulence Interactions and Consequences for Cloud Physics, Bull. Amer. Meteor. Soc., 81, 285–298, 2000.

Vaillancourt, P. A., Yau, M. K., and Grabowski, W. W.: Microscopic Approach to Cloud Droplet Growth by Condensation. Part I: Model Description and Results without Turbulence, J. Atmos. Sci., 58, 1945–1964, 2001.

25 Vaillancourt, P. A., Yau, M. K., Bartello, P., and Grabowski, W. W.: Microscopic Approach to Cloud Droplet Growth by Condensation. Part II: Turbulence, Clustering, and Condensational Growth, J. Atmos. Sci., 59, 3421–3435, 2002.

Wang, L.-P., Ayala, O., Kasprzak, S. E., and Grabowski, W. W.: Theoretical Formulation of Collision Rate and Collision Efficiency of Hydrodynamically Interacting Cloud Droplets in Turbulent Atmosphere, J. Atmos. Sci., 62, 2433–2450, 2005.

Wang, L.-P., Ayala, O., Rosa, B., and Grabowski, W. W.: Turbulent collision efficiency of heavy particles relevant to cloud droplets, New J.
30 Phys., 10, 075 013, 2008.